STATE OF THE CLIMATE IN 2015

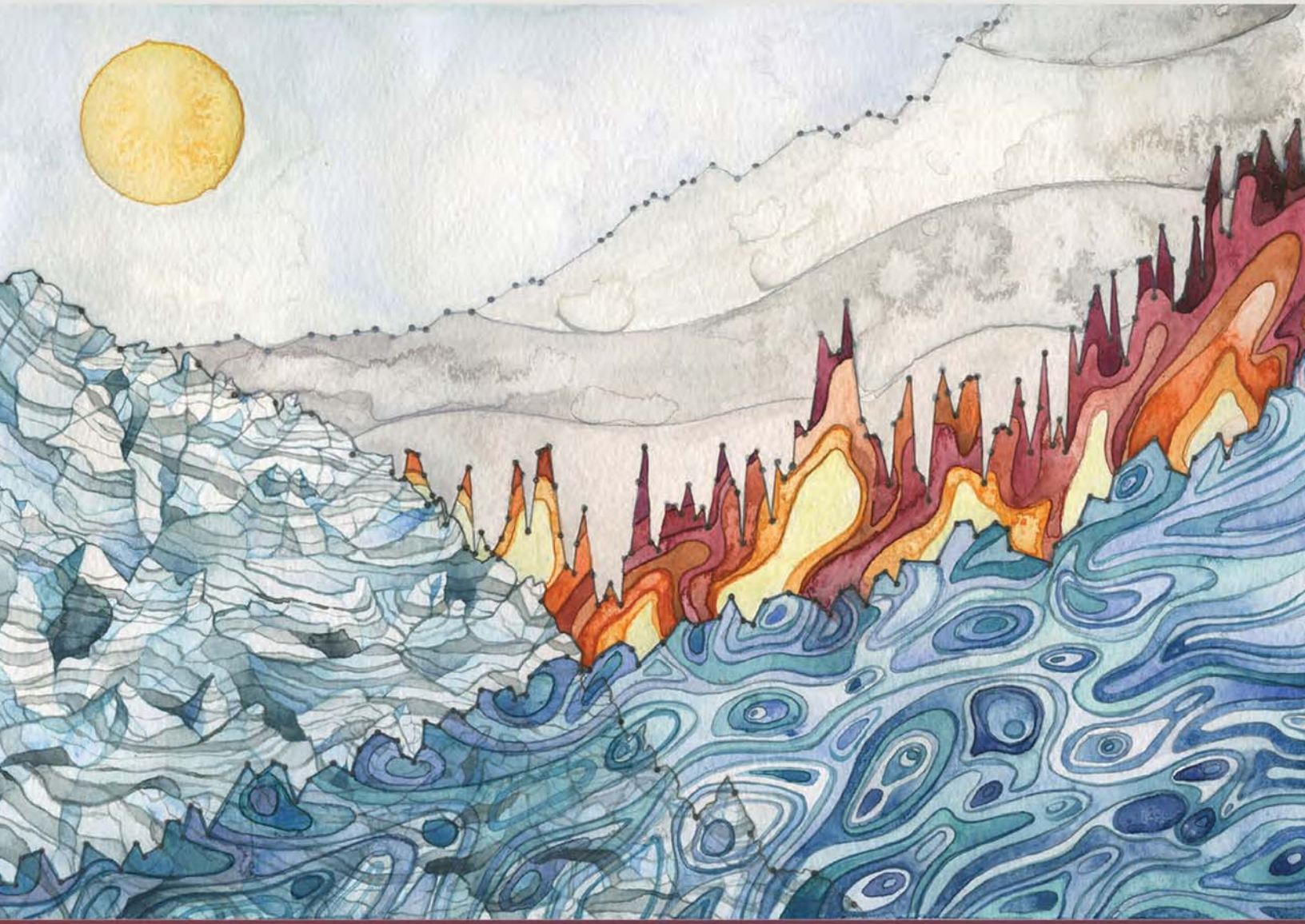

Special Supplement to the
Bulletin of the American Meteorological Society
Vol. 97, No. 8, August 2016

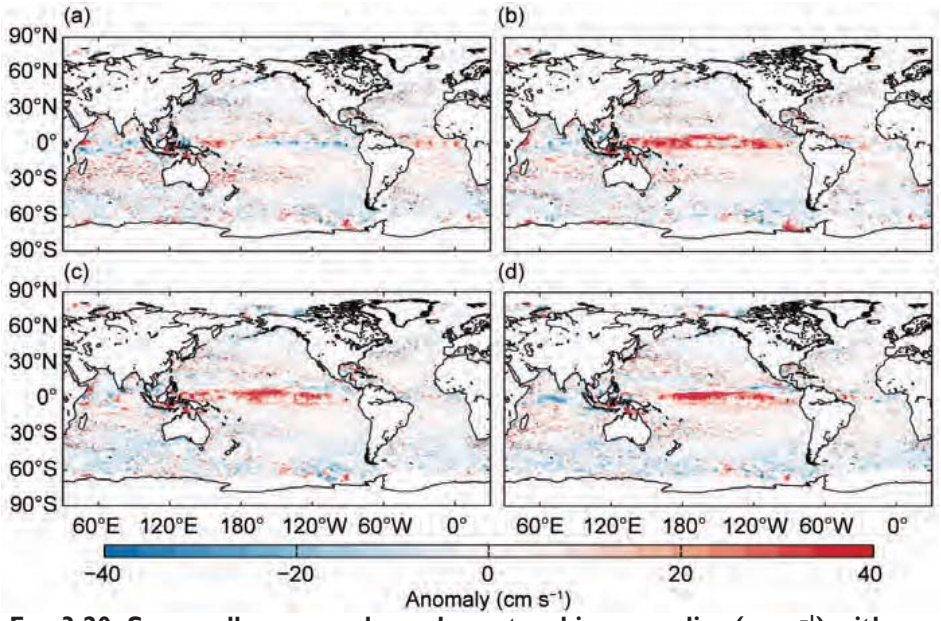

Fig. 3.20. Seasonally averaged zonal geostrophic anomalies (cm s^{-1}) with respect to seasonal climatology, for (a) Dec 2014–Feb 2015, (b) Mar–May 2015, (c) Jun–Aug 2015, and (d) Sep–Nov 2015.

zonal current tendencies in the Indian Ocean basin (Fig. 3.19b). In 2015, the strongest anomalies with respect to monthly climatology were seen in October and November, with an unusually early development of the North Monsoon Current (e.g., Beal et al. 2013) associated with westward anomalies of ~30 cm s^{-1} at 3°S–2°N, 60°–80°E during these months (Fig. 3.20d). Large-scale current anomalies returned to near-climatological December values by the end of 2015.

The Agulhas Current transport is a key indicator of Indian–Atlantic Ocean interbasin water exchanges. The annual mean transport of the Agulhas Current has been decreasing from a high set in 2013, with values of 56 Sv in 2013 (1 Sv $\equiv 10^6$ m^3 s^{-1}), 53 Sv in 2014, and 50 Sv in 2015. The 2015 transport of 50 Sv is equal to the Agulhas' long-term (1993–2015) mean.

Annual mean anomalies in the Atlantic Ocean (Fig. 3.19a) indicate a 5–7 cm s^{-1} strengthening of the eastward NECC at 4.5°–6.5°N, 30°–50°W, and conditions close to climatology along the equator. However, the annual average hides a pattern of reversing equatorial anomalies between boreal winter and spring (Fig. 3.20). The year began with eastward anomalies of 20 cm s^{-1} from 3°S to 2°N across much of the basin, which weakened through February and were present only at 25°–35°W in March/April. In May, westward anomalies of 10–15 cm s^{-1} developed across the basin from 2°S to 2°N. These anomalies weakened considerably through June and were no longer present in July. No significant basinwide equatorial anomalies were seen in the remainder of 2015.

The Gulf Stream in 2015 remained close to its climatological position with little change from 2014 (Fig. 3.19).

The North Brazil Current, which sheds rings that carry waters from the Southern Hemisphere into the North Atlantic and has important ecosystem impacts downstream (Kelly et al. 2000), exhibited an annual transport smaller than its long-term (1993–2015) value. As in 2014, it shed eight rings in 2015, a larger-than-average value. Sea level anomalies in the region, which have generally increased since 2001 (apart from lows in 2003 and 2008), remained higher than average in 2015.

In the southwest Atlantic Ocean, the Brazil Current carries waters from subtropical to subpolar regions, mainly in the form of large anticyclonic rings (Lentini et al. 2006). The separation of the Brazil Current front from the continental shelf break continued to exhibit a seasonal cycle, which is mainly driven by wind stress curl variations and the transport of this current. During 1993–98, the annual mean separation of the front shifted southward in response to a long-term warming in South Atlantic temperatures (cf. Lumpkin and Garzoli 2010; Goni et al. 2011). In 2015, the Brazil Current front and its separation from the continental shelf break persisted south of its mean position, unchanged from 2014.

h. Meridional overturning circulation observations in the North Atlantic Ocean—M. O. Baringer, M. Lankhorst, D. Volkov, S. Garzoli, S. Dong, U. Send, and C. S. Meinen

This section describes the Atlantic meridional overturning circulation (AMOC) and the Atlantic meridional heat transport (AMHT), determined by the large-scale ocean circulation wherein northward moving upper layer waters are transformed into deep waters that return southward, redistributing heat, freshwater, carbon, and nutrients. Previous *State of the Climate* reports (e.g., Baringer et al. 2013) and reviews (e.g., Srokosz and Bryden 2015; Perez et al. 2015; Carton et al. 2014; Srokosz et al. 2012) discuss the AMOC's impact on climate variability and ecosystems. The AMOC is computed as the maximum of the

vertical accumulation of the horizontally integrated velocity across a section (i.e., the maximum transport that occurs in either the upper or lower layer before the circulation starts to change direction again). The AMHT involves the co-variability of temperature and velocity and is only meaningful as a flux (and hence, independent of the absolute temperature scale used) when the total mass transport can be accounted for (i.e., sums to zero). Observing systems can measure both temperature and velocity, usually with tradeoffs in system design that favor the computation of one quantity over the other. Here we describe the AMOC from observing systems at 41°N, 26°N, and 16°N, and AMHT at 41°N, 26°N, and 35°S. In the future, AMOC observing systems in the South Atlantic and subpolar North Atlantic should provide additional time series (e.g., Srokosz et al. 2012).

The longest time series of ocean transport to serve as an index of the AMOC's strength in the North Atlantic (e.g., Frajka-Williams 2015; Duchez et al. 2014) is from the Florida Current (FC, as the Gulf Stream is called at 26°N), measured since 1982 (Fig. 3.22). FC and AMOC transport variations at all time scales also are inversely linked to sea level variations along the east coast (Goddard et al. 2015; McCarthy et al. 2015). The median 1982–2015 transport of the FC is 31.9 ± 0.25 Sv (one standard error of the mean assuming a 20-day integral time scale) with a small downward trend of −0.31 ± 0.26 Sv decade^{-1} (errors estimating 95% significance as above). The 2015 median FC transport was 31.7 ± 1.7 Sv, only slightly below the long-term average. Daily FC transports compared to those of all previous years (Fig. 3.22) indicate that

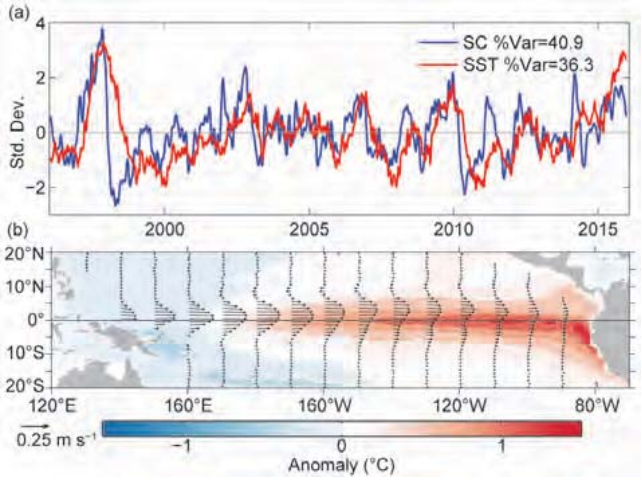

Fig. 3.21. EOF of surface current (SC) and SST anomaly variations in the tropical Pacific from the OSCAR model (Bonjean and Lagerloef 2002; www.esr.org /enso_index.html). (a) EOF Amplitude time series normalized by their respective standard deviations. (b) EOF Spatial structures.

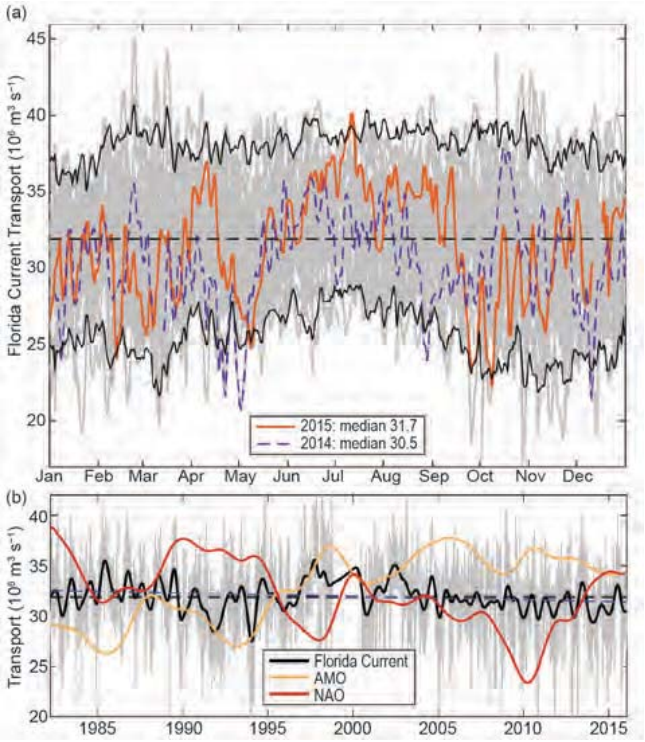

Fig. 3.22. (a) Daily estimates of Florida Current transport (10^6 m^3 s^{-1}) during 2015 (orange solid line), 2014 (dashed purple line), and 1982–2012 (light gray lines) with 95% confidence interval of daily transport values computed from all years (black solid line) and the long-term mean (dashed black). (b) Daily estimates of Florida Current transport (10^6 m^3 s^{-1}) for the full time series record (light gray), smoothed using a 12-month second-order Butterworth filter (heavy black line), mean transport for the full record (dashed black line), and linear trend from 1982 through 2015 (dashed blue line). Two-year low-passed Atlantic Multidecadal (AMO, yellow line) and North Atlantic Oscillation (NAO, red line) indices are also shown.

2015, like 2014, had several unusually low transport anomalies (extremes defined as outside the 95% confidence limits for daily values). These occurred during 8–9 May, 24–29 September, and 5–9 October 2015. The lowest daily 2015 FC transport was 22.2 Sv on 8 October, with transports < 23 Sv for five days around this date. During 2015 there was only one high transport event, with an average transport of > 39 Sv from 8 to 13 July.

At 41°N, a combination of profiling Argo floats (that measure ocean temperature and salinity for the upper 2000 m on broad spatial scales, as well as velocity at 1000 m) and altimetry-derived surface velocity (Willis and Fu 2008) are used to estimate the AMOC (Fig. 3.23) and AMHT (Fig. 3.24). This time series has not been updated since last year's report (Baringer et al. 2015a,b), extending from January 2002 to December 2014. At 26°N, the AMOC/AMHT (Figs. 3.23 and 3.24) is measured with full-water column moorings

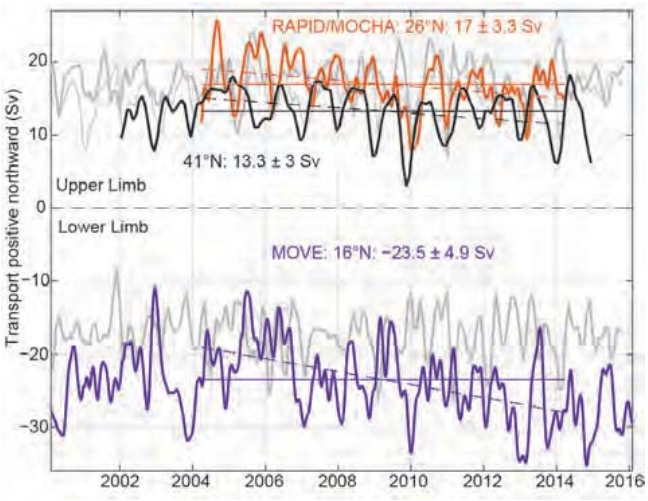

Fig. 3.23. Estimates of Atlantic meridional overturning circulation (1 Sv ≡ 10^6 m^3 s^{-1}; AMOC) from the Argo/Altimetry estimate at 41°N (black; Willis 2010), the RAPID-MOC/MOCHA/WBTS 26°N array (red; McCarthy et al. 2015), and the German/NOAA MOVE array at 16°N (blue; Send et al. 2011) shown versus year. All time series have a three-month second-order Butterworth low-pass filter applied. Horizontal lines are mean transports during similar time periods as listed in the corresponding text. Dashed lines are trends for each series over the same time period. For MOVE data, the net zonal and vertical integral of the deep circulation represents the lower limb of the AMOC (with a negative sign indicating southward flow), and hence a stronger negative (southward) flow represents an increase in the AMOC amplitude. Light gray lines show ECCO2-derived transports: (top) thin gray is the 41°N transport, thick gray is the 26°N transport, (bottom) shows the negative meridional overturning circulation in the model for ease of comparison with the 16°N data.

that span the full basin and include direct transport measurements in the boundary currents as part of the large RAPID-MOC/MOCHA/WBTS 26°N mooring array (Smeed et al. 2015). The data from these moorings are collected every 18 months, most recently in December 2015; too late to be calibrated and finalized for this report. The 26°N data shown here extend from April 2004 to March 2014 (see last year's report for full details). At 16°N, a mooring array of inverted echo sounders, current meters, and dynamic height moorings (Send et al. 2011) measures the flow below 1000 m (the southward flowing part of the AMOC "conveyor belt") that sends North Atlantic Deep Water toward the equator; hence, the AMOC estimate at this latitude (Fig. 3.23) is a negative number (southward deep flow) to distinguish these observations from the full water column systems. Since this array only measures the deep circulation, an estimate of the AMHT is impossible at 16°N because of the missed large signals and high correlations in the surface waters. These data have been updated since last year's report and now extend from February 2000 to February 2016. At 35°S in the South Atlantic, the AMHT (Fig. 3.24) is estimated using a combination of high-density (closely spaced) expendable bathythermograph (XBT) and broader-scale Argo profiling float data (Garzoli et al. 2012). While the AMOC has also been estimated at 35°S (e.g., Dong et al. 2009), those estimates (not shown) are rough because the XBTs only extend to 750 m. These data are collected and analyzed in near–real time, with values spanning July 2002 to October 2015.

Some guidance on 2015 AMOC and AMHT variability can be gained from state estimation model output, constrained by observations. February 1992–November 2015 monthly estimates of AMOC and AMHT from the global MITgcm in ECCO2 (cube-sphere) configuration (e.g., Menemenlis et al. 2008), forced with the new JRA-55 atmospheric fields (Kobayashi et al. 2016) and GPCP precipitation

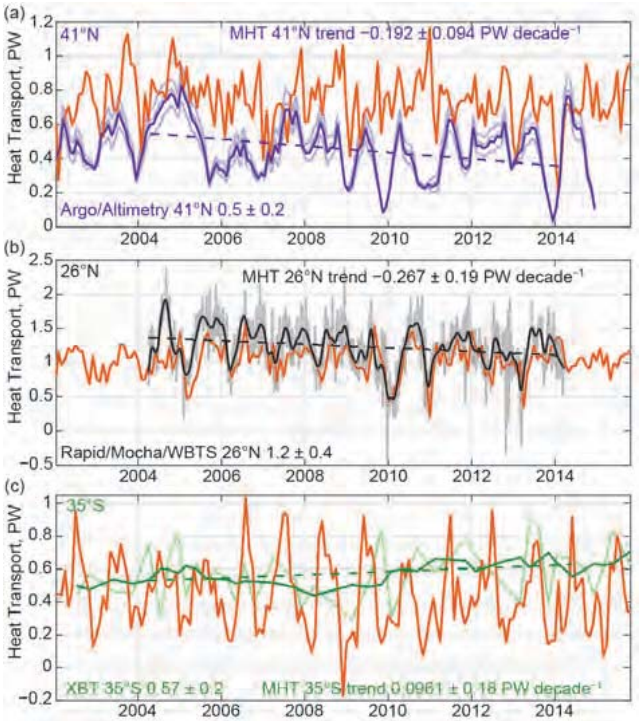

Fig. 3.24. Observed time series of Atlantic meridional heat transport (PW; AMHT) at (a) 41°N (from profiling floats following Hobbs and Willis 2012; blue lines), with uncertainties (light blue lines) and the trend (dashed blue line), at (b) 26°N (from mooring/hydrography data) 12-hourly values (gray line), filtered with a 3-month low-pass filter (black line), and the trend (black dashed line), and at (c) 30°–35°S (from XBTs) quarterly values (light green), filtered with yearly boxcar (dark green line), and the trend (dashed green line). Heat transports simulated by ECCO2 (orange lines) are shown at all latitudes.

(Huffman et al. 2012), are analyzed here. The ECCO2 model output is well correlated with the instrument-based measurement of the AMOC (Fig. 3.23) and AMHT (Fig. 3.24) at 26°N and 41°N, with correlations of 0.58/0.59 and 0.57/0.38, respectively, all significantly above the 95% confidence level. ECCO2 model output is not statistically significantly correlated with the 16°N AMOC or 35°S AMHT transports (correlation values of 0.12 and 0.13, respectively). At 26°N and 41°N the AMOC and AMHT in the ECCO2 output show a slight increase from 17.6 Sv and 1.02 PW (1 PW = 10^{15} W) in 2014 to 18.3 Sv and 1.09 PW in 2015. Preliminary analysis of the new data from 26°N (not shown) indicates that the transport has continued fairly unchanged since 2011 (through December 2015), with values lower than the earlier part of the record (D. A. Smeed, 2016, personal communication). Additionally, there is no unusual "event" in the assimilation time series, as has been clearly seen in other time periods (e.g., Fig. 3.24). This finding is supported by the FC time series and the ECCO2 state estimation (Fig. 3.22).

At 16°N, the time series of the AMOC estimate decreased from 29.0 Sv in 2013, to 28.4 Sv in 2014, and to 27.2 Sv in 2015 (as stated earlier the decrease in southward flow implies an increase in the AMOC at this latitude; Fig. 3.23). This reduction has led to a reduced estimate of the long-term trend of the AMOC from February 2000 to February 2016 at 16°N to be +3.6 Sv ± 2.5 Sv decade^{-1}. This trend is of the opposite sign from the trends at 26°N and 41°N (–4.1 ± 3.2 Sv decade^{-1} and –1.3 ± 4.9 Sv decade^{-1}). A similar situation exists with the 35°S AMHT transport estimate. In the south, the AMHT has remained essentially constant for the last three years (mean value 0.6 PW northward). This implies a virtually steady AMOC as well (the AMOC and AMHT being highly correlated). This recently constant AMHT has reduced the long-term trend of an increasing AMHT to +0.11 ± 0.10 PW decade^{-1}. From these data it is clear that the variability at all latitudes in the Atlantic is not well correlated and, therefore, data from more than one latitude are needed to describe the state of the ocean.

i. Global ocean phytoplankton—B. A. Franz, M. J. Behrenfeld, D. A. Siegel, and S. R. Signorini

Marine phytoplankton represent roughly half the net primary production (NPP) on Earth, fixing atmospheric CO_2 into food that fuels global ocean ecosystems and drives biogeochemical cycles (e.g., Field et al. 1998; Falkowski et al. 1998). Satellite ocean color sensors, such as SeaWiFS (McClain 2009), MODIS (Esaias et al. 1998), and VIIRS (Oudrari et al. 2014), provide observations of sufficient frequency and geographic coverage to globally monitor changes in the near-surface concentrations of the phytoplankton pigment chlorophyll-*a* (Chl*a*; mg m^{-3}). Chl*a* provides a first-order index of phytoplankton abundance and is proportional to the maximum sunlight energy absorbed for photosynthesis (Behrenfeld et al. 2006). Here, global Chl*a* distributions for 2015 are evaluated within the context of the 18-year continuous record provided through the combined observations of SeaWiFS (1997–2010), MODIS on *Aqua* (MODISA, 2002–present), and VIIRS on *Suomi-NPP* (2011–present). All Chl*a* data used in this analysis correspond to version R2014.0 (http://oceancolor.gsfc.nasa.gov/cms/reprocessing/), which uses common algorithms and calibration methods to maximize consistency in the multimission satellite record.

The spatial distribution of VIIRS annual mean Chl*a* for 2015 (Fig. 3.25) is generally consistent with the well-established, physically driven distribution of nutrients (e.g., Siegel et al. 2013). To assess changes in Chl*a* for 2015, mean values for VIIRS Chl*a* in each month of 2015 were subtracted from monthly climatological means for MODISA (2003–2011) within globally distributed geographic bins, and then those monthly anomaly fields were averaged (Fig. 3.26a). Identical calculations were performed on MODISA SST (°C) data to produce a companion SST annual mean anomaly (Fig. 3.26b).

In 2015, the phytoplankton Chl*a* concentrations across much of the equatorial Pacific were strongly depressed, with concentrations 20%–50% below the climatological norm. This response is generally corre-

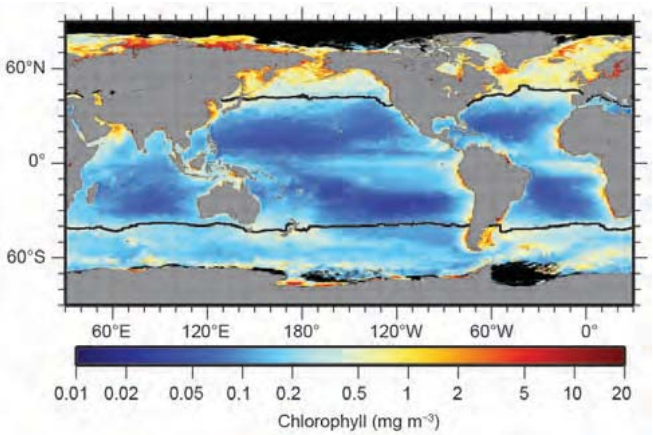

Fig. 3.25. Mean 2015 Chl*a* distribution (mg m^{-3}) derived from VIIRS with the location of the mean 15°C SST isotherm (black lines) delineating boundaries of the permanently stratified ocean (PSO). Chl*a* data are from NASA Reprocessing version 2014.0. Data are averaged into geo-referenced equal area bins of approximately 4.6 km × 4.6 km and mapped to an equi-rectangular projection centered at 150°W.